Fabrication of Photoswitchable and Thermotunable Multicolor Fluorescent Hybrid Silica Nanoparticles Coated with Dye-Labeled Poly(*N*-isopropylacrylamide) Brushes

Tao Wu, Gang Zou, Jinming Hu, and Shiyong Liu*

CAS Key Laboratory of Soft Matter Chemistry, Department of Polymer Science and Engineering, Hefei National Laboratory for Physical Sciences at the Microscale, University of Science and Technology of China, Hefei, Anhui 230026, China

We report on the fabrication of hybrid silica nanoparticles densely grafted with thermoresponsive poly(*N*-isopropylacrylamide) (PNIPAM) brushes with inner and outer layers selectively labeled with fluorescence resonance energy transfer (FRET) donors, 4-(2-acryloyloxyethylamino)-7-nitro-2,1,3-benzoxadiazole (NBDAE), and photoswitchable acceptors, 1′-(2-methacryloxyethyl)-3′,3′-dimethyl-6-nitro-spiro(2*H*-1-benzo-pyran-2,2′-indoline) (SPMA), respectively, via surface-initiated sequential atom transfer radical polymerization (ATRP). P(NIPAM-*co*-NBDAE)-*b*-P(NIPAM-*co*-SPMA) brushes at the surface of silica core exhibit collapse in the broad temperature range of 20−37 °C. UV irradiation of the aqueous dispersion of hybrid silica nanoparticles induces the transformation of SPMA moieties in the outer layer of polymer brushes from nonfluorescent spiropyran (SP) form to fluorescent merocyanine (MC) form, leading to occurrence of the FRET process between NBDAE and SPMA residues. Most importantly, the FRET efficiency can be facilely tuned via thermo-induced collapse/swelling of P(NIPAM-*co*-NBDAE)-*b*-P(NIPAM-*co*-SPMA) brushes by changing the relative distance between donor and acceptor species located within the inner and outer layers of polymer brushes, respectively. Thus, hybrid silica nanoparticles coated with P(NIPAM-*co*-NBDAE)-*b*-P(NIPAM-*co*-SPMA) brushes can serve as a sensitive ratiometric fluorescent thermometer. On the other hand, when the hybrid nanoparticle dispersion was irradiated with visible light again after UV irradiation, the MC form of SPMA moieties reverts back to the nonfluorescent SP form, leading to the turn-off of FRET process. Overall, aqueous dispersion of this novel type of hybrid silica nanoparticle is capable of emitting multicolor fluorescence, which can be facilely tuned by UV irradiation, visible light, and temperatures or a proper combination of these factors.

Introduction

In the past decade, fluorescent thermometers based on small molecules[1−12] and polymers[13−24] have received considerable interest due to their capability of monitoring temperatures in microscopic domains (cells and microfluidic devices) or hostile environments (high-voltage or microwave irradiation), where conventional thermometry is getting impractical. In terms of water-soluble polymeric fluorescent thermometers, thermoresponsive poly(*N*-isopropylacrylamide) (PNIPAM) randomly labeled with polarity-sensitive dyes, such as benzofurazan,[14−17,22] hemicyanine,[20] carbazole,[24] and dicyanomethylene-4*H*-pyran derivatives,[23] have

*To whom correspondence should be addressed. Email: sliu@ustc.edu.cn.
(1) Schrum, K. F.; Williams, A. M.; Haerther, S. A.; Benamotz, D. *Anal. Chem.* **1994**, *66*, 2788–2790.
(2) Lou, J. F.; Hatton, T. A.; Laibinis, P. E. *Anal. Chem.* **1997**, *69*, 1262–1264.
(3) Engeser, M.; Fabbrizzi, L.; Licchelli, M.; Sacchi, D. *Chem. Commun.* **1999**, 1191–1192.
(4) Chandrasekharan, N.; Kelly, L. A. *J. Am. Chem. Soc.* **2001**, *123*, 9898–9899.
(5) Ross, D.; Gaitan, M.; Locascio, L. E. *Anal. Chem.* **2001**, *73*, 4117–4123.
(6) Lupton, J. M. *Appl. Phys. Lett.* **2002**, *81*, 2478–2480.
(7) Baker, G. A.; Baker, S. N.; McCleskey, T. M. *Chem. Commun.* **2003**, 2932–2933.
(8) Huang, J.; Peng, A. D.; Fu, H. B.; Ma, Y.; Zhai, T. Y.; Yao, J. N. *J. Phys. Chem. A* **2006**, *110*, 9079–9083.
(9) Baleizao, C.; Nagl, S.; Borisov, S. M.; Schaferling, M.; Wolfbeis, O. S.; Berberan-Santos, M. N. *Chem.—Eur. J.* **2007**, *13*, 3643–3651.
(10) Crenshaw, B. R.; Kunzelman, J.; Sing, C. E.; Ander, C.; Weder, C. *Macromol. Chem. Phys.* **2007**, *208*, 572–580.
(11) Davis, R.; Das, S. *J. Fluoresc.* **2005**, *15*, 749–753.
(12) Sakakibara, J.; Adrian, R. J. *Exp. Fluids* **1999**, *26*, 7–15.
(13) Wong, F. H. C.; Banks, D. S.; Abu-Arish, A.; Fradin, C. *J. Am. Chem. Soc.* **2007**, *129*, 10302–10303.
(14) Uchiyama, S.; Matsumura, Y.; de Silva, A. P.; Iwai, K. *Anal. Chem.* **2003**, *75*, 5926–5935.
(15) Uchiyama, S.; Matsumura, Y.; de Silva, A. P.; Iwai, K. *Anal. Chem.* **2004**, *76*, 1793–1798.
(16) Uchiyama, S.; Kawai, N.; de Silva, A. P.; Iwai, K. *J. Am. Chem. Soc.* **2004**, *126*, 3032–3033.
(17) Iwai, K.; Matsumura, Y.; Uchiyama, S.; de Silva, A. P. *J. Mater. Chem.* **2005**, *15*, 2796–2800.
(18) Kwak, G.; Fukao, S.; Fujiki, M.; Sakaguchi, T.; Masuda, T. *Chem. Mater.* **2006**, *18*, 2081–2085.
(19) Shiraishi, Y.; Miyamoto, R.; Zhang, X.; Hirai, T. *Org. Lett.* **2007**, *9*, 3921–3924.
(20) Shiraishi, Y.; Miyamoto, R.; Hirai, T. *Langmuir* **2008**, *24*, 4273–4279.
(21) Hong, S. W.; Kim, D. Y.; Lee, J. U.; Jo, W. H. *Macromolecules* **2009**, *42*, 2756–2761.
(22) Gota, C.; Okabe, K.; Funatsu, T.; Harada, Y.; Uchiyama, S. *J. Am. Chem. Soc.* **2009**, *131*, 2766–2767.
(23) Guo, Z. Q.; Zhu, W. H.; Xiong, Y. Y.; Tian, H. *Macromolecules* **2009**, *42*, 1448–1453.
(24) Yan, Q.; Yuan, J. Y.; Yuan, W. Z.; Zhou, M.; Yin, Y. W.; Pan, C. Y. *Chem. Commun.* **2008**, 6188–6190.

Scheme 1. Schematic Illustration of ATRP Synthesis of Hybrid Silica Nanoparticles Coated with Thermoresponsive P(NIPAM-*co*-NBDAE)-*b*-P(NIPAM-*co*-SPMA) Brushes with the Inner and Outer Layers Selectively Labeled with Fluorescence Resonance Energy Transfer (FRET) Donor (NBDAE) and Photoswitchable Acceptor (SPMA) Residues, Respectively
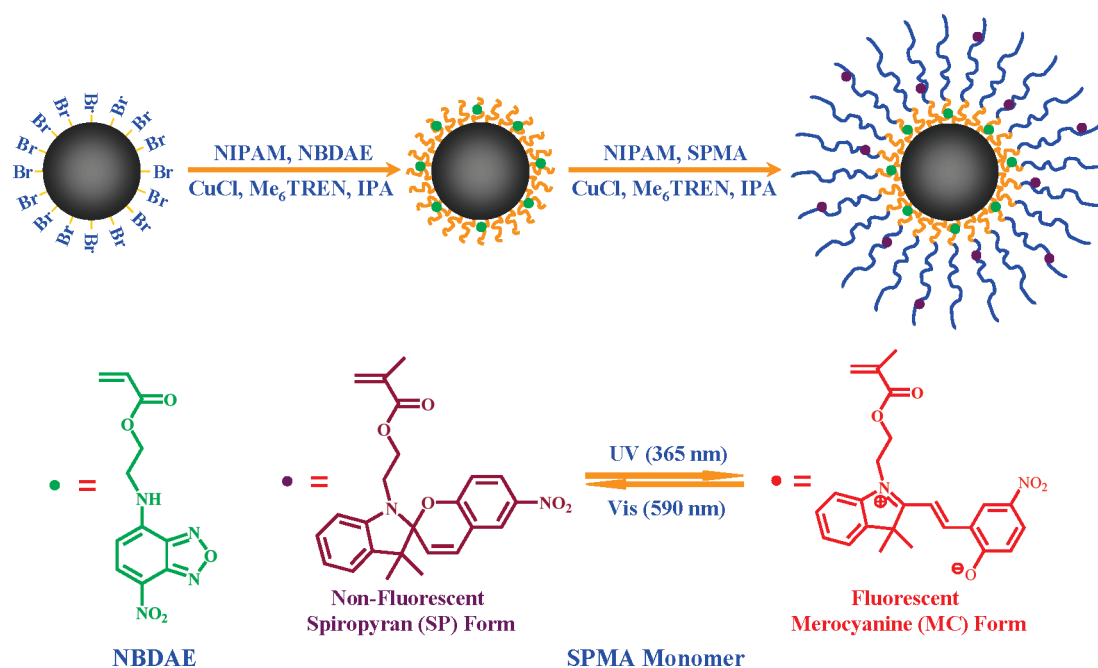
been extensively investigated. In a recent example, Jo et al.[21] synthesized linear pyrene-terminated PNIPAM with one C_{60} moiety labeled at the other chain end or at the middle of the chain. The relative distance between C_{60} and pyrene considerably decreases upon heating above the lower critical solution temperature (LCST) of PNI-PAM, leading to enhanced quenching of pyrene fluorescence emission by C_{60}. It should be noted that the above PNIPAM-based fluorescent thermometers can only be applied to a relatively narrow temperature range, as uncontrolled aggregation or even macroscopic phase separation will occur at elevated temperatures due to the LCST phase behavior of PNIPAM. To circumvent this problem, Uchiyama et al.[16,17] have ingeniously co-polymerized hydrophilic or even ionic monomers into dye-labeled PNIPAM, aiming to broaden the range of detection temperatures.

It is worthy to note that in all of the above examples, the enhancing or quenching of fluorescence emission intensity, i.e., the change of relative fluorescence intensity, has been employed to determine temperatures, which can be significantly affected by local dye concentrations, background noises, and measuring conditions. To solve this issue, ratiometric thermometers based on the comparison of emissions at different wavelengths have been proposed, and a few successful examples of small molecule-based systems were reported.[8,12] Lyon et al.[25] selectively labeled the core and shell region of PNIPAM microgels with fluorescent donor and acceptor residues. Upon heating, the collapse of core−shell microgels can enhance the fluorescence resonance energy transfer (FRET) efficiency. In another example, they simultaneously labeled

the core region of core−shell PNIPAM microgels with FRET donors and acceptors, Cy5 and Cy5.5, focusing on investigation of the restriction exerted by the shell layer on the swelling/collapse of microgel cores.[26] Theoretically, these two examples can be considered as prototypes of microgel-based ratiometric FRET thermometers.

In the past few years, optical imaging of living cells with fluorescent polymeric nanoparticles (NPs) has aroused a great deal of interest.[27] Compared to small molecule dyes, fluorescent NPs are bright and photostable and prove to be a robust platform for the incorporation of diverse functionalities. Nanoparticles with photoswitchable fluorescence emission on the basis of spiropyran derivatives have also been reported.[28−34] The spiropyran moiety adopts the colorless spiropyran (SP) form in the dark or under visible light (vis), whereas it spontaneously converts to the colored and fluorescent merocyanine (MC) form upon UV irradiation (Scheme 1).

In a notable example, Li et al.[31] incorporated spiropyr-an dyes into polymeric latex particles. The aqueous

(25) Gan, D. J.; Lyon, L. A. *J. Am. Chem. Soc.* **2001**, *123*, 8203–8209.

(26) Jones, C. D.; McGrath, J. G.; Lyon, L. A. *J. Phys. Chem. B* **2004**, *108*, 12652–12657.
(27) Douma, K.; Prinzen, L.; Slaaf, D. W.; Reutelingsperger, C. P. M.; Biessen, E. A. L.; Hackeng, T. M.; Post, M. J.; van Zandvoort, M. *Small* **2009**, *5*, 544–557.
(28) Zhu, L. Y.; Wu, W. W.; Zhu, M. Q.; Han, J. J.; Hurst, J. K.; Li, A. D. Q. *J. Am. Chem. Soc.* **2007**, *129*, 3524–3526.
(29) Zhu, L. Y.; Zhu, M. Q.; Hurst, J. K.; Li, A. D. Q. *J. Am. Chem. Soc.* **2005**, *127*, 8968–8970.
(30) Medintz, I. L.; Trammell, S. A.; Mattoussi, H.; Mauro, J. M. *J. Am. Chem. Soc.* **2004**, *126*, 30–31.
(31) Zhu, M. Q.; Zhu, L. Y.; Han, J. J.; Wu, W. W.; Hurst, J. K.; Li, A. D. Q. *J. Am. Chem. Soc.* **2006**, *128*, 4303–4309.
(32) Chen, J.; Zeng, F.; Wu, S. Z.; Zhao, J. Q.; Chen, Q. M.; Tong, Z. *Chem. Commun.* **2008**, 5580–5582.
(33) Chen, J.; Zeng, F.; Wu, S. Z.; Chen, Q. M.; Tong, Z. *Chem.—Eur. J.* **2008**, *14*, 4851–4860.
(34) Emin, S. M.; Sogoshi, N.; Nakabayashi, S.; Fujihara, T.; Dushkin, C. D. *J. Phys. Chem. C* **2009**, *113*, 3998–4007.

dispersion emits bright red fluorescence upon UV irradiation and becomes nonfluorescent upon vis irradiation. Compared to single color fluorescent nanoparticles, photoswitchable dual ones are more desirable because they can distinguish themselves from the emission of background fluorophores. The same research group has also introduced FRET donor species, perylene derivatives, and spiropyran acceptors into latex particles, and photoswitching between green and red fluorescence can be facilely achieved via UV/vis irradiation. These dual-color fluorescent nanoparticles based on the photoswitchable FRET process were then used in cell imaging.[28] Later on, Wu et al.[32,33] synthesized amphiphilic core−shell nanoparticles covalently attached with spiropyran moieties. After solubilization with hydrophobic nitrobenzoxadiazloyl (NBD) derivatives within the hydrophobic core, reversible photoswiching between green and red fluorescence emission has also been realized.

However, the imprecise locating and slow release of embedded NBD dyes might be disadvantageous considering the long-term emission stability.

On the basis of past experiences with stimuli−responsive polymers and microgels, we figure out that the combination of photoswitchable FRET systems with organic/inorganic hybrid nanoparticles coated with responsive polymer brushes should be able to provide extra advantages, such as structural stability, tunable FRET efficiency, and multicolor fluorescence. In this work, we report on the fabrication of hybrid silica nanoparticles densely grafted with thermoresponsive PNIPAM brushes with inner and outer layers selectively labeled with fluorescence resonance energy transfer (FRET) donors, 4-(2-acryloyloxyethylamino)-7-nitro-2,1,3-benzoxadiazole (NBDAE), and photoswitchable acceptors, 1′-(2-methacryloxyethyl)-3′,3′-dimethyl-6-nitro-spiro(2H-1-benzo-pyran-2,2′-indoline) (SPMA), respectively, via

Scheme 2. (a) Schematic Illustration for the Reversible Modulation of a Multicolor Fluorescent System Fabricated from Hybrid Silica Nanoparticles Coated with Thermoresponsive P(NIPAM-*co*-NBDAE)-*b*-P(NIPAM-*co*-SPMA) Brushes, in Which the FRET Process Can Be Switched on or off via UV or Vis Irradiation and the FRET Efficiency Can Be Tuned via Thermo-induced Collapse/Swelling of Responsive Polymer Brushes (b) Photographs Immediately Recorded under a 365 nm UV Lamp at Varying Conditions: (1) 20 °C, upon Vis Irradiation, (2) 20 °C, upon UV Irradiation, (3) 35 °C, upon Vis Irradiation, and (4) 35 °C, upon UV Irradiation[a]
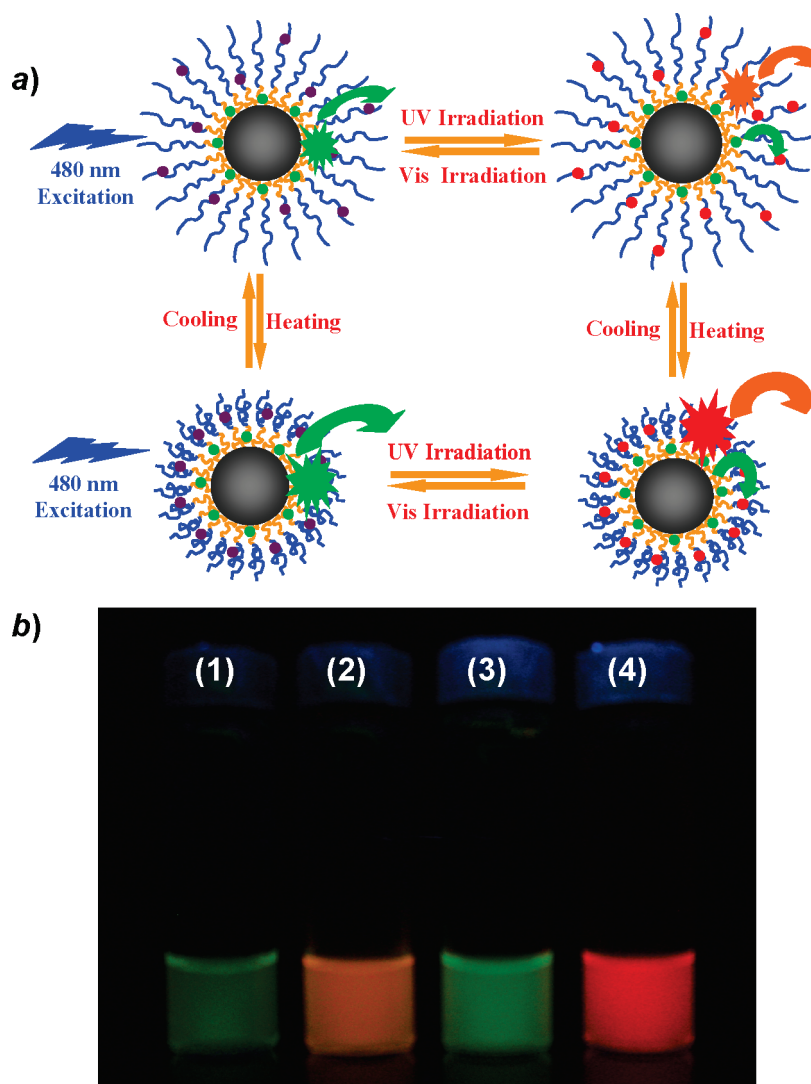
[a] The duration of UV or vis irradiation is 4 min in all cases.

surface-initiated sequential atom transfer radical polymerization (ATRP) (Scheme 1). P(NIPAM-*co*-NBDAE)-*b*-P(NIPAM-*co*- SPMA) brushes at the surface of silica core exhibit collapse in the broad temperature range of 20–37 °C. UV irradiation of the aqueous dispersion of hybrid silica nanoparticles induces the transformation of SPMA moieties in the outer layer of the polymer brush from the nonfluorescent spiropyran (SP) form to the fluorescent merocyanine (MC) form, leading to occurrence of a FRET process between NBDAE and SPMA residues. Most importantly, the FRET efficiency can be facilely tuned via thermo-induced collapse/swelling of P(NIPAM-*co*-NBDAE)-*b*-P(NIPAM-*co*-SPMA) brushes by changing the relative distance between donor and acceptor species located within the inner and outer layer of polymer brushes, respectively. The aqueous dispersion of this novel type of hybrid silica nanoparticles is capable of emitting multicolor fluorescence, which can be facilely tuned by UV irradiation, visible light, and temperatures or a proper combination of these factors (Scheme 2).

Experimental Section

Materials. *N*-Isopropylacrylamide (NIPAM, 97%, Tokyo Kasei Kagyo Co.) was purified by recrystallization from the mixture of benzene and *n*-hexane (1/3 v/v). CuCl (99.999%), CuCl$_2$ (99%), and 2-bromoisobutyryl bromide (97%) were purchased from Aldrich and used without further purification. 4-Chloro-7-nitrobenzofurazan (NBD-Cl, 99%), 2,3,3-trimethylindolenine (98%), and 5-nitrosalicylaldehyde (98%) were purchased from Alfa and used as received. Tetraethoxysilane (TEOS) and 3-aminopropyl-triethoxysilane (APTES) were purchased from Silicone Materials Co. (Wuhan Univ.) and distilled under reduced pressure just prior to use. Tris-(2-(dimethylamino)ethyl)amine (Me$_6$TREN) and 2-bromoisobutyrate-functionalized silica nanoparticles were synthesized according to literature procedures.[35,36] All other reagents were purchased from Sinopharm Chemical Reagent Co. Ltd. and used as received.

Sample Preparation. General approaches employed for the preparation of hybrid silica nanoparticles coated with P(NIPAM-*co*-NBDAE)-*b*-P(NIPAM-*co*-SPMA) brushes are shown in Scheme 1.

Synthesis of SPMA Monomer. 1′-(2-Hydroxyethyl)-3′,3′-dimethyl-6-nitrospiro(2*H*-1-benzopyran-2,2′-indoline) (SP-OH) was prepared according to literature procedures.[37] Typical procedures employed for the preparation of SPMA are as follows. A mixture containing SP-OH (1.0 g, 2.84 mmol), Et$_3$N (500 μL, 3.6 mmol), and dry CH$_2$Cl$_2$ (15 mL) was cooled to 0 °C under N$_2$ atmosphere and protection against visible light exposure. Methacryloyl chloride (340 μL, 3.5 mmol) in dry CH$_2$Cl$_2$ (5 mL) was then added dropwise over 0.5 h. After stirring for 10 h at room temperature, the solvent was removed using a rotary evaporator. The residues were purified by silica gel column chromatography (100−200 mesh) using CH$_2$Cl$_2$/petroleum ether (2:1 v/v) as eluent. The yield was 0.4 g pale green crystals in 33% yield. ^{1}H NMR (400 MHz CDCl$_3$) δ (ppm): 1.16

(s, 3H), 1.28 (s, 3H), 1.92 (s, 3H), 3.38−3.62 (m, 2H), 4.3 (t, 2H), 5.56 and 6.07 (d, 2H), 5.87 (d, 1H), 6.73 (q, 2H) 6.89 (q, 2H), 7.09 (d, 1H), 7.17−7.23 (m, 1H), 7.96−8.05 (m, 2H) (Figure S1a of the Supporting Information).

Synthesis of NBDAE Monomer. 4-(2-Acryloyloxyethylamino)-7-nitro-2,1,3-benzoxa-diazole (NBDAE) was synthesized according to slightly modified literature procedures.[14] In a typical run, 4-(2-hydroxyethylamino)-7-nitro-2,1,3-benzoxa-diazole[38] (200 mg, 0.89 mmol) was dissolved in acetonitrile (60 mL), followed by the dropwise addition of acryloyl chloride (4 mL, 50 mmol). The reaction mixture was refluxed for 4 h. The solvent was removed under reduced pressure, and the residues were purified by silica gel column chromatography using CH$_2$Cl$_2$ as the eluent. The yield was 150 mg orange powder in 60% yield. ^{1}H NMR (400 MHz, CDCl$_3$) δ (ppm): 8.50 (1H, d), 6.63 (1H, br), 6.49 (1H, d), 6.26 (1H, d), 6.16 (1H, dd), 5.94 (1H, d), 4.56 (2H, t), 3.84 (2H, m) (Figure S1b of the Supporting Information).

Surface-Initiated ATRP of NIPAM and NBDAE from 2-Bromoisobutyrate-Functionalized Silica Nanoparticles. Into a Schlenk flask equipped with a magnetic stir bar initiator-functionalized silica nanoparticles (400 mg, 0.060 mmol initiator), Me$_6$TREN (59 mg, 0.26 mmol), CuCl$_2$ (5.3 mg, 0.04 mmol), NBDAE (21 mg, 0.075 mmol), NIPAM (2.7 g, 23.9 mmol), and 2-propanol (8 mL) were charged. After ultrasonication for 5 min, the mixture was degassed by one freeze−pump−thaw cycle. CuCl (20 mg, 0.20 mmol) was then introduced under protection of N$_2$ flow. The reaction flask was subjected to two additional freeze−pump−thaw cycles and then placed in an oil bath thermostatted at 25 °C. After stirring for 1.5 h, the reaction flask was opened, exposed to air, diluted with 2-propanol, and followed by the addition of CuCl$_2$ (300 mg, 2.23 mmol). Hybrid nanoparticles were isolated via centrifugation at ∼15 000*g* for 1 h and then washed with ethanol. The above centrifugation−washing cycle was repeated three times. The obtained hybrid silica nanoparticles coated with P(NIPAM-*co*-NBDAE) brushes were dried in a vacuum oven overnight at room temperature. A portion of the obtained hybrid silica nanoparticles were dispersed in THF via ultrasonication. P(NIPAM-*co*-NBDAE) brushes were then cleaved from silica cores via etching with aqueous solution of hydrofluoric acid (HF, 47 wt %) for GPC measurement (***Caution! HF is extremely corrosive, and all operations with aqueous HF should be conducted with suitable personal protective equipment***).

Surface-Initiated ATRP of NIPAM and SPMA from Hybrid Silica Nanoparticles Coated with P(NIPAM-co-NBDAE) Brushes. Hybrid silica nanoparticles coated with P(NIPAM-*co*-NBDAE) brushes (100 mg, 0.0025 mmol initiator), Me$_6$TREN (25 mg, 0.11 mmol), CuCl$_2$ (2 mg, 0.015 mmol), NIPAM (1.0 g, 8.84 mmol), SPMA (6 mg, 0.014 mmol), and 2-propanol (4 mL) were charged into a Schlenk flask equipped with a magnetic stir bar. The reaction mixture was degassed by one freeze−pump−thaw cycle. CuCl (7 mg, 0.071 mmol) was then introduced under protection of N$_2$ flow. The reaction flask was then subjected to two additional freeze−pump−thaw cycles and immersed into an oil bath thermostatted at 25 °C. After stirring for 7 h, the flask was opened, exposed to air, and diluted with 2-propanol. Hybrid nanoparticles were isolated via centrifugation at ∼15 000*g* for 1 h and washed with ethanol. The above centrifugation−washing cycle was repeated three times. The obtained hybrid silica nanoparticles coated with

(35) Ciampolini, M.; Nardi, N. *Inorg. Chem.* **1966**, *5*, 41–44.
(36) Wu, T.; Zhang, Y. F.; Wang, X. F.; Liu, S. Y. *Chem. Mater.* **2008**, *20*, 101–109.
(37) Raymo, F. M.; Giordani, S. *J. Am. Chem. Soc.* **2001**, *123*, 4651–4652.
(38) Onoda, M.; Uchiyama, S.; Santa, T.; Imai, K. *Anal. Chem.* **2002**, *74*, 4089–4096.

3792 *Chem. Mater., Vol. 21, No. 16, 2009*

Wu et al.

P(NIPAM-*co*-NBDAE)-*b*-P(NIPAM-*co*-SPMA) brushes were dried in a vacuum oven overnight at room temperature.

Characterization. *Gel Permeation Chromatography*. Molecular weights and molecular weight distributions were determined by gel permeation chromatography (GPC) equipped with a Waters 1515 pump and Waters 2414 differential refractive index detector (set at 30 °C). It used a series of two linear Styragel columns (HR2 and HR4) at an oven temperature of 45 °C. The eluent was THF at a flow rate of 1.0 mL/min. A series of low polydispersity polystyrene standards were employed for GPC calibration.

Fourier Transform Infrared Spectroscopy. Fourier transform infrared (FT-IR) spectra were recorded on a Bruker VECTOR-22 IR spectrometer. The spectra were collected at 64 scans with a spectral resolution of 4 cm^{-1}.

NMR Spectroscopy. All NMR spectra were recorded on a Bruker AV400 NMR spectrometer (resonance frequency of 400 MHz for ^{1}H) operated in the Fourier transform mode. CDCl$_3$ was used as the solvent.

Thermogravimetric Analysis (*TGA*). TGA was performed in air using a Perkin-Elmer Diamond TG/DTA at a heating rate of 10 °C/min over the temperature range from room temperature to 700 °C.

High-Resolution Transmission Electron Microscopy (*HRTEM*). HRTEM observations were conducted on a JEOL 2010 electron microscope. The sample for HRTEM observations was prepared by placing 10 μL nanoparticle solution on copper grids successively coated with thin films of Formvar and carbon. No staining was required.

Laser Light Scattering (*LLS*). A commercial spectrometer (ALV/DLS/SLS-5022F) equipped with a multitau digital time correlator (ALV5000) and a cylindrical 22 mW UNIPHASE He−Ne laser (λ_0 = 632 nm) as the light source was employed for dynamic and static LLS measurements. In dynamic LLS, scattered light was collected at a fixed angle of 90° for a duration of 15 min. Distribution averages and particle size distributions were computed using cumulants analysis and CONTIN routines. All data were averaged over three measurements.

UV−vis Absorption Measurements. UV−vis absorption of aqueous dispersion of hybrid silica nanoparticles was acquired on a Unico UV/vis 2802PCS spectrophotometer.

Fluorescence Measurements. Fluorescence spectra were recorded on an Aminco-Bowman Series 2 (AB2) spectrofluorometer (Thermo Spectronic). The temperature of the water-jacketed cell holder was controlled by a programmable circulation bath. The slit widths were set at 4 nm for excitation and 4 nm for emission. The UV (365 nm, 15 W) and light-emitting diode (LED) lamps (588−595 nm, 50 W) were used as light sources for UV and visible light irradiation, respectively. Fluorescent microscopy images of the aqueous dispersion of hybrid silica nanoparticles coated with P(NIPAM-*co*-NBDAE)-*b*-P(NIP-AM-*co*-SPMA) brushes were recorded on a Olympus FV-1000 confocal laser scanning microscope (CLSM). The sample was excited at 488 nm, and fluorescence signals were collected at 500−535 and 580−680 nm through different fluorescence channels.

Results and Discussion

Hybrid Silica Nanoparticles Coated with Thermoresponsive P(NIPAM-*co*-NBDAE)-*b*-P(NIPAM-*co*-SPMA) Brushes. Previously, we have reported the preparation of hybrid silica NPs coated with PNIPAM brushes via
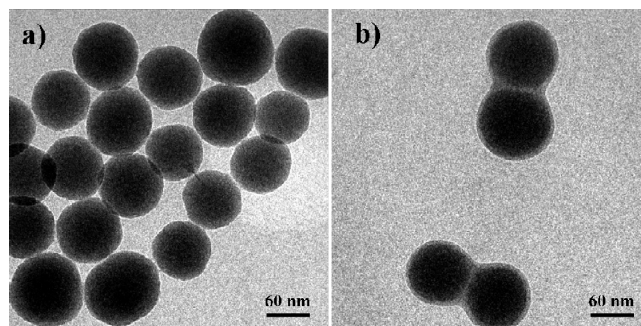

Figure 1. HRTEM images obtained for (a) 2-bromoisobutyrate-functionalized silica nanoparticles and (b) hybrid silica nanoparticles coated with P(NIPAM-*co*-NBDAE)-*b*- P(NIPAM-*co*-SPMA) brushes.

surface-initiated ATRP and investigated the thermal phase transition behavior of PNIPAM brushes at the surface of silica NPs.[36] In the current work, general approaches employed for the preparation of hybrid silica nanoparticles coated with thermoresponsive P(NIPAM-*co*-NBDAE)-*b*-P(NIPAM-*co*-SPMA) brushes are shown in Scheme 1.

2-Bromoisobutyrate-functionalized silica nanoparticles were synthesized according to procedures employed in the previous work,[36] which can be summarized as follows. Bare silica nanoparticles were prepared via the Stöber process,[39] which were then modified with APTES to afford amino-functionalized silica nanoparticles. 2-Bromoisobutyrate-functionalized silica nanoparticles were prepared via the amidation of amino-functionalized silica nanoparticles with 2-bromoisobutyryl bromide. 2-Bromoisobutyrate-functionalized silica NPs were characterized by FT-IR analysis; the presence of amide moieties can be evidenced by the presence of the amide II band (1540 cm^{-1}, N−H stretching) (Figure S2b of the Supporting Information), as compared to that of bare silica NPs (Figure S2a). The average radius of initiator-functionalized silica nanoparticles is determined to be ∼45 nm by HRTEM (Figure 1a). Thermogravimetric analysis (TGA) reveals an ∼2.0 wt % difference in weight retentions at 650 °C between amino- and 2-bromoisobutyrate-functionalized silica nanoparticles (Figure S3 of the Supporting Information). If the mass retention of amino-functionalized silica nanoparticles at 650 °C is used as the reference and the density of the silica nanoparticles is assumed to be identical to that of bulk silica (2.07 g/cm^3), we can roughly estimate the grafting density of ATRP initiators at the surface of silica nanoparticles to be ∼0.31 nm^2/initiator.

The preparation of hybrid silica nanoparticles coated with P(NIPAM-*co*-NBDAE)-*b*-P(NIPAM-*co*-SPMA) chains was performed by sequential surface-initiated ATRP (Scheme 1).[40−42] Hybrid silica nanoparticles coated with P(NIPAM-*co*-NBDAE) brushes were

(39) Stober, W.; Fink, A.; Bohn, E. *J. Colloid Interface Sci.* **1968**, *26*, 62–69.
(40) Wang, B. B.; Li, B.; Zhao, B.; Li, C. Y. *J. Am. Chem. Soc.* **2008**, *130*, 11594–11595.
(41) Li, D. J.; Zhao, B. *Langmuir* **2007**, *23*, 2208–2217.
(42) Li, D. J.; Jones, G. L.; Dunlap, J. R.; Hua, F. J.; Zhao, B. *Langmuir* **2006**, *22*, 3344–3351.

prepared at first by the ATRP of NIPAM and NBDAE (0.31 mol % relative to NIPAM) from the surface of 2-bromoisobutyrate-functionalized silica nanoparticles. $CuCl_2$ (20 mol % relative to CuCl) was added in order to ensure an efficient exchange between the dormant and active species to control the polymerization. Hybrid silica nanoparticles coated with P(NIPAM-*co*-NBDAE)-*b*-P-(NIPAM-*co*-SPMA) chains were then obtained by the ATRP chain extension of P(NIPAM-*co*-NBDAE) brushes at the surface of hybrid silica nanoparticles with NIPAM and SPMA (0.16 mol % relative to NIPAM) comonomers via surface-initiated ATRP.

Figure 1b shows the HRTEM image of hybrid silica nanoparticles coated with P(NIPAM-*co*-NBDAE)-*b*-P(NIPAM-*co*-SPMA) brushes. It is clearly evident that silica cores are surrounded by a polymer layer with a thickness of about 8 nm. The successful chain extension was confirmed by GPC analysis for P(NIPAM-*co*-NBDAE) and P(NIPAM-*co*-NBDAE)-*b*-P(NIPAM-*co*-SPMA) brushes cleaved from hybrid silica NPs via etching with hydrofluoric acid, revealing an M_n of 6.0 kDa and an M_w/M_n of 1.15 for the former and an M_n of 22.0 kDa and an M_w/M_n of 1.30 for the latter (Figure 2). Compared to that of P(NIPAM-*co*-NBDAE), a higher polydispersity and the slight tailing at the low M_w side for P(NIPAM-*co*-NBDAE)-*b*-P(NIPAM-*co*-SPMA) suggested the presence of some uninitiated chains during the ATRP chain extension. A similar phenomenon has been previously reported by Pyun et al. for sequential ATRP from silica NPs.[43] Figure S2 (of the Supporting Information) also shows the FT-IR spectra of hybrid silica nanoparticles coated with P(NIPAM-*co*-NBDAE) and P(NIPAM-*co*-NBDAE)-*b*-P(NIPAM-*co*-SPMA) brushes, respectively. The amide I band (1650 cm^{-1}, C=O stretching) and amide II band (1550 cm^{-1}, N—H stretching) characteristic of amide moieties in PNIPAM can be clearly observed in both cases. No absorbance bands characteristic of NBDAE or SPMA moieties can be discerned, probably due to their relatively low contents.

From the TGA results shown in Figure S3d and e (of the Supporting Information), the weight retentions at 650 °C obtained for hybrid silica nanoparticles coated with P(NIPAM-*co*-NBDAE) and P(NIPAM-*co*-NBD-AE)-*b*-P(NIPAM-*co*-SPMA) brushes are 73.9% and 55.3%, respectively. The weight fraction of P(NIPAM-*co*-NBDAE) and P(NIPAM-*co*-NBDAE)-*b*- P(NIPAM-*co*-SPMA) brushes within hybrid silica NPs are calculated to be ~15.2% and 36.5%, respectively. When amino-functionalized silica NPs were used as the reference, the grafting density of P(NIPAM-*co*-NBDAE) and P(NIPAM-*co*-NBDAE)-*b*-P(NIPAM-*co*-SPMA) chains at the surface of silica nanoparticles can be estimated to be 1.53 and 1.84 nm^2/chain, respectively, based on procedures employed in relevant literature reports.[36,44] As
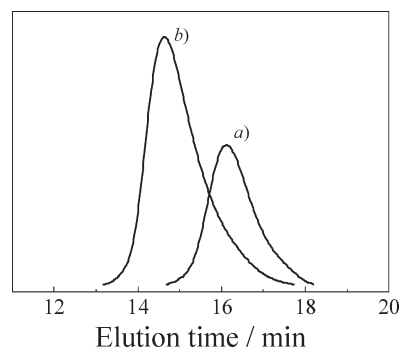

Figure 2. GPC traces obtained for (a) P(NIPAM-*co*-NBDAE) and (b) P(NIPAM-*co*- NBDAE)-*b*-P(NIPAM-*co*-SPMA) cleaved from hybrid silica nanoparticles coated with P(NIPAM-*co*-NBDAE) and P(NIPAM-*co*-NBDAE)-*b*-P(NIPAM-*co*-SPMA) brushes, respectively, via etching with hydrofluoric acid.

the grafting density of ATRP initiators is 0.31 nm^2/ initiator, the initiating efficiency for surface-initiated ATRP in the first and second step can be roughly estimated to be ~20% and 17%, respectively.

It can also be calculated that the average distance between neighboring grafted P(NIPAM-*co*-NBDAE)-*b*-P(NIPAM-*co*-SPMA) chains at the surface of silica nanoparticles is about ~1.4 nm. The degree of the polymerization (DP) of grafted P(NIPAM-*co*-NBDAE)-*b*-P(NIPAM-*co*-SPMA) chains is ca. 194. Preliminary experiments revealed that hydrodynamic dimensions of the free PNIPAM chain with a DP of ~194 in aqueous solution (6−8 nm) are much larger than the average distance between neighboring grafted chains with comparable DPs (~1.3 nm), indicating that the grafted P(NIPAM-*co*-NBDAE)-*b*-P(NIPAM-*co*-SPMA) layer falls into the brush regime. Thus, grafted chains in the polymer brushes are crowded and forced to stretch away from the substrate due to steric exclusion between neighboring chains.

Dynamic LLS was employed to characterize temperature-dependent size changes of hybrid silica nanoparticles grafted with thermoresponsive P(NIPAM-*co*-NBDAE)-*b*-P(NIPAM-*co*-SPMA) brushes in aqueous solution (Figure 3). It is well-known that PNIPAM homopolymer undergoes a coil-to-globule phase transition in dilute aqueous solution at its LCST of ca. 32 °C.[45] At temperatures below the LCST, PNIPAM chains adopt a random-coil conformation; whereas at temperatures above the LCST, hydrogen bonding interactions between water molecules and amide moieties are disrupted, leading to chain collapse and aggregation.[46] Upon heating, $\langle R_h \rangle$ decreases monotonically from 85 to 76 nm in the temperature range of 20−29 °C and, then, exhibits a further decrease from 76 nm at 29 °C to 61.5 nm at 37 °C. The above results agree quite well with our previous report concerning PNIPAM brush-coated silica NPs.[36] This also suggests that the incorporation of NBDAE and SPMA moieties into the inner and outer layer of PNIPAM

(43) Pyun, J.; Jia, S. J.; Kowalewski, T.; Patterson, G. D.; Matyjaszewski, K. *Macromolecules* **2003**, *36*, 5094–5104.
(44) Luzinov, I.; Julthongpiput, D.; Malz, H.; Pionteck, J.; Tsukruk, V. V. *Macromolecules* **2000**, *33*, 1043–1048.

(45) Schild, H. G. *Prog. Polym. Sci.* **1992**, *17*, 163–249.
(46) Ahmed, Z.; Gooding, E. A.; Pimenov, K. V.; Wang, L. L.; Asher, S. A. *J. Phys. Chem. B* **2009**, *113*, 4248–4256.
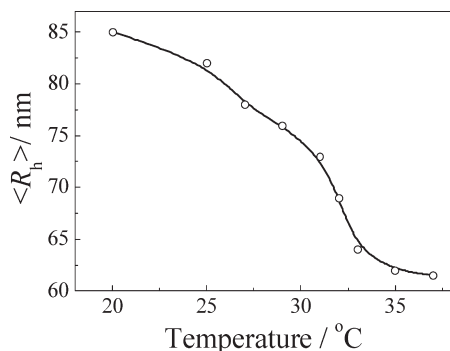
Figure 3. Temperature dependence of intensity-averaged hydrodynamic radius, $\langle R_h \rangle$, obtained for the aqueous dispersion (0.05 g/L) of hybrid silica nanoparticles coated with P(NIPAM-*co*-NBDAE)-*b*-P(NIPAM-*co*-SPMA) brushes.

brushes does not alter the thermoresponsive collapsing behavior. On the other hand, though SPMA moieties in P(NIPAM-*co*-NBDAE)-*b*-P(NIPAM-*co*-SPMA) brushes can transform from nonpolar SP form to zwitterionic MC form after UV irradiation, further LLS experiments reveal that the $\langle R_h \rangle$ values of hybrid nanoparticles exhibit no discernible changes before and after UV irradiation in the temperature range of 20−37 °C.

In the past decade, the phase transition behavior of PNIPAM brushes anchored at the surface of flat or spherical substrates has been investigated experimentally and theoretically.[47−55] PNIPAM chains in polymer brushes are crowded and forced to stretch away from the substrate due to steric exclusion between neighboring chains, and the inner layer of PNIPAM brushes is more crowded than the outer part due to higher chain density in the former, leading to broad phase transition ranges.[50−54]

Tenhu et al.[55] reported that PNIPAM brushes on the surface of gold nanoparticles undergo two well-separated thermal phase transitions, as evidenced by microcalorimetry measurements. Previously, we also observed the double thermal phase transition behavior of PNIPAM brushes grafted at the surface of silica nanoparticles.[36] In the current case, the continuous decrease of $\langle R_h \rangle$ in the broad temperature range of 20−37 °C for hybrid silica nanoparticles coated with P(NIPAM-*co*-NBDAE)-*b*-P(NIPAM-*co*-SPMA) brushes agrees reasonably with previous literature reports.[36,55]

Photoswitchable and Thermotunable Multicolor Fluorescence Emission of Hybrid Nanoparticles. It has been

(47) Binkert, T.; Oberreich, J.; Meewes, M.; Nyffenegger, R.; Ricka, J. *Macromolecules* **1991**, *24*, 5806–5810.
(48) Zhulina, E. B.; Borisov, O. V.; Pryamitsyn, V. A.; Birshtein, T. M. *Macromolecules* **1991**, *24*, 140–149.
(49) Wagner, M.; Brochardwyart, F.; Hervet, H.; Degennes, P. G. *Colloid Polym. Sci.* **1993**, *271*, 621–628.
(50) Balamurugan, S.; Mendez, S.; Balamurugan, S. S.; O'Brien, M. J.; Lopez, G. P. *Langmuir* **2003**, *19*, 2545–2549.
(51) Yim, H.; Kent, M. S.; Huber, D. L.; Satija, S.; Majewski, J.; Smith, G. S. *Macromolecules* **2003**, *36*, 5244–5251.
(52) Yim, H.; Kent, M. S.; Mendez, S.; Balamurugan, S. S.; Balamurugan, S.; Lopez, G. P.; Satija, S. *Macromolecules* **2004**, *37*, 1994–1997.
(53) Liu, G. M.; Zhang, G. Z. *J. Phys. Chem. B* **2005**, *109*, 743–747.
(54) Annaka, M.; Yahiro, C.; Nagase, K.; Kikuchi, A.; Okano, T. *Polymer* **2007**, *48*, 5713–5720.
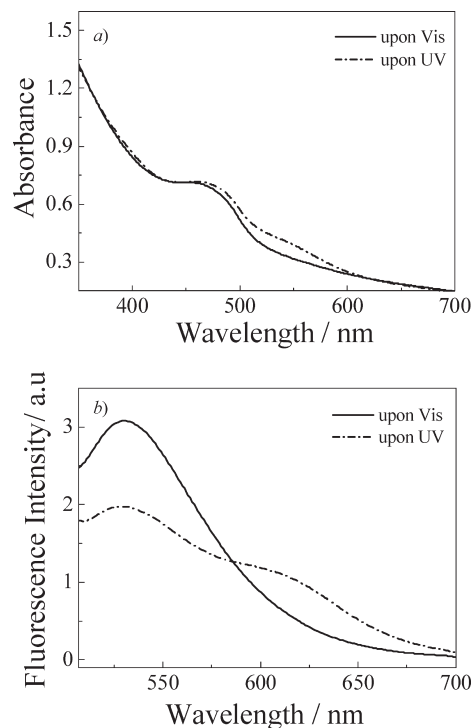(55) Shan, J.; Chen, J.; Nuopponen, M.; Tenhu, H. *Langmuir* **2004**, *20*, 4671–4676.

Figure 4. (a) Absorption spectra and (b) fluorescence emission spectra (λ_{ex} = 480 nm; slit widths: ex 4 nm, em 4 nm) recorded for the aqueous dispersion (0.25 g/L, 20 °C) of hybrid silica nanoparticles coated with P(NIPAM-*co*-NBDAE)-*b*-P(NIPAM-*co*-SPMA) brushes upon visible and UV light irradiation for 4 min, respectively.

well-documented that spiropyran moieties adopt ring-closed nonpolar SP form under visible light and transform into ring-opened zwitterionic MC form upon UV irradiation (Scheme 1).[56] The SP form is colorless with nonfluorescent, whereas the MC form exhibits an absorbance band in the range of 500−600 nm and fluorescence emission at 620 nm. Figure 4a shows the absorption spectra of the aqueous dispersion of hybrid silica nanoparticles coated with P(NIPAM-*co*-NBDAE)-*b*-P-(NIPAM-*co*-SPMA) brushes upon visible and UV irradiation at 20 °C. Upon visible light irradiation, spiropyran moieties in polymer brushes are in the SP form; we can only discern an absorbance band at 470 nm, which is ascribed to NBDAE moieties. After UV irradiation, a new absorbance band in the range of 520 to 600 nm can be observed, which can be ascribed to the ring-opened MC form of SPMA residues.

Figure 4b shows fluorescence emission spectra of the aqueous dispersion of hybrid silica nanoparticles at 20 °C upon visible and UV light irradiation, respectively. When excited at 480 nm, only fluorescence emission of NBDAE moieties with a maximum at 530 nm can be observed for hybrid NP dispersion under vis irradiation (Scheme 2). It is worth noting that the emission band of NBDAE residues (500−620 nm) generally matches the absorbance band of the MC form of SPMA moieties (520−600 nm), thus the FRET process between the NBDAE and MC forms of SPMA can occur if they are spatially close to each other (< ∼10 nm).

(56) Berkovic, G.; Krongauz, V.; Weiss, V. *Chem. Rev.* **2000**, *100*, 1741–1753.

Article

Chem. Mater., Vol. 21, No. 16, 2009 3795

Upon UV irradiation, hybrid silica NP dispersion exhibits a new emission band at around 618 nm, which can be attributed to the MC form of SPMA residues. On the other hand, the fluorescence intensity at 530 nm of NBDAE residues considerably decreases, as compared to that before UV irradiation (Figure 4b). This can be ascribed to the quenching of NBDAE fluorescence by the MC form of SPMA moieties, i.e., the FRET process occurs. Figure S4 (of the Supporting Information) shows fluorescent microscopy images of the aqueous dispersion of hybrid silica nanoparticles coated with P(NIPAM-*co*-NBDAE)-*b*-P(NIPAM-*co*-SPMA) brushes. Upon vis irradiation, strong green fluorescence (500−535 nm) and quite weak red emission (580−680 nm) from hybrid nanoparticles were observed (Figure S4A and B). Upon UV irradiation, we can apparently observe enhanced red fluorescence emission accompanied with decreased green fluorescence emission (Figure S4C and D). These results are in agreement with those obtained from fluorescence measurements (Figure 4b). From Scheme 2b, we can also discern an apparent green to orange fluorescence emission for hybrid NP dispersions under UV 365 nm irradiation.

Figure 5a shows typical fluorescence response behavior of the aqueous dispersion of hybrid silica NPs coated with P(NIPAM-*co*-NBDAE)-*b*-P(NIPAM-*co*-SPMA) brushes upon irradiation with UV and vis irradiation at 20 °C. Upon irradiation with UV at 365 nm, the fluorescence intensity of NBDAE moieties at 530 nm abruptly decreases within 2 min and then stabilizes out, indicating its quenching by the ring-opened MC form of SPMA. Upon irradiation with 590 nm light, the NBDAE fluorescence can almost recover to the original value within 10 min. In agreement with previous reports by Wu et al.,[32,33] the FRET process between NBDAE and SPMA residues can be reversibly switched on and off via cycled irradiation with UV 365 nm and vis 590 nm (Figure 5b, Scheme 2). After five cycles, we can notice a slight decrease of NBDAE fluorescence intensity under vis irradiation conditions, indicating the presence of irreversible photodamage to NBDAE and spiropyran moieties under repeated UV irradiation.[57]

It is well-known that the FRET efficiency strongly depends on the relative distance between fluorescent donors and acceptors, the decrease of which can considerably improve the FRET efficiency.[58] In the next sections, we will discuss the thermotunable FRET process and photoswitchable multicolor fluorescence emission from hybrid silica NPs coated with thermoresponsive P(NIPAM-*co*-NBDAE)-*b*-P(NIPAM-*co*-SPMA) brushes.

Temperature-dependent fluorescence results of hybrid silica NPs coated with P(NIPAM-*co*-NBDAE) and P-(NIPAM-*co*-NBDAE)-*b*-P(NIPAM-*co*-SPMA) brushes are shown in Figures 6 and 7. Under visible light condi-
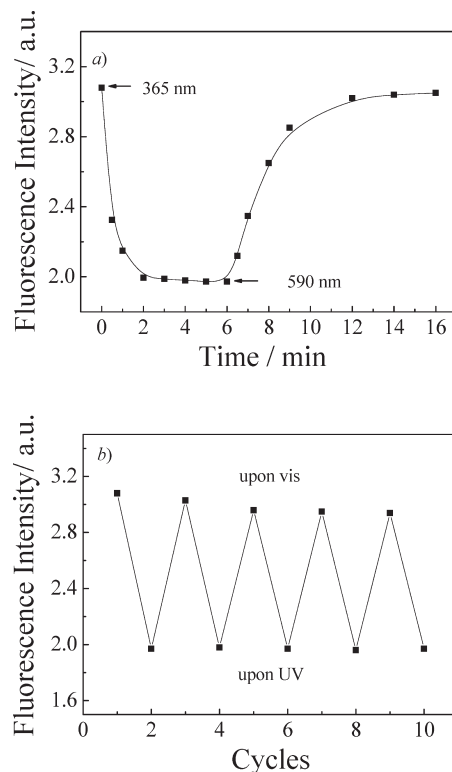
(57) Such, G.; Evans, R. A.; Yee, L. H.; Davis, T. P. *J. Macromol. Sci.−Polym. Rev.* **2003**, *C43*, 547–579.
(58) Farinha, J. P. S.; Martinho, J. M. G. *J. Phys. Chem. C* **2008**, *112*, 10591–10601.

Figure 5. (a) Fluorescence response (λ_{ex} = 480 nm and λ_{em} = 530 nm; slit widths: ex 4 nm, em 4 nm) of aqueous dispersion (0.25 g/L, 20 °C) of hybrid silica nanoparticles coated with P(NIPAM-*co*-NBDAE)-*b*-P(NIPAM-*co*-SPMA) brushes on irradiation with 365 nm UV and then 590 nm visible light and (b) fluorescence intensity changes of the dispersion after UV illumination and visible light irradiation cycles.
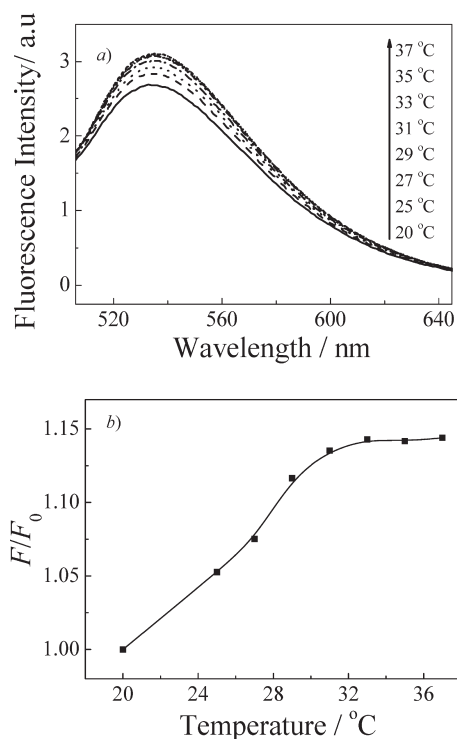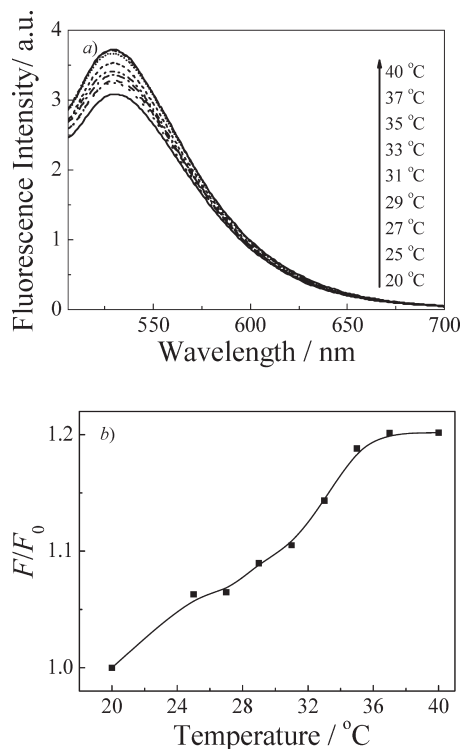

Figure 6. (a) Fluorescence spectra (λ_{ex} = 480 nm; slit widths: ex 4 nm, em 4 nm) and (b) change in relative fluorescence intensity (λ_{em} = 530 nm) obtained in the temperature range of 20−37 °C for the aqueous dispersion (0.25 g/L) of hybrid silica nanoparticles coated with P(NIPAM-*co*-NBDAE) brushes.

Figure 7. (a) Fluorescence spectra (λ_{ex} = 480 nm; slit widths: ex 4 nm, em 4 nm) and (b) change in relative fluorescence intensity (λ_{em} = 530 nm) obtained in the temperature range of 20−37 °C for the aqueous dispersion (0.25 g/L) of hybrid silica nanoparticles coated with P(NIPAM-*co*-NBDAE)-*b*-P(NIPAM-*co*-SPMA) brushes.

Figure 8. (a) Fluorescence spectra (λ_{ex} = 480 nm; slit widths: ex 4 nm, em 4 nm) and (b) fluorescence intensity ratio changes, F_{618}/F_{530}, in the temperature range of 20−37 °C obtained for the aqueous dispersion (0.25 g/L) of hybrid silica nanoparticles coated with P(NIPAM-*co*-NBDAE)-*b*-P(NIPAM-*co*-SPMA) brushes immediately upon 365 nm UV irradiation for 4 min.

tions, only NBDAE residues can exhibit fluorescence emission. Thermo-induced collapse of polymer brushes results in a more hydrophobic environment, and this will enhance the fluorescence of NBDAE moieties. A similar phenomenon was reported by Uchiyama et al.[14] for NBD-labeled linear PNIPAM samples, which can serve as fluorescent thermometers at around the thermal phase transition temperature range. Possessing a DP of ∼53, P(NIPAM-*co*-NBDAE) brush-coated silica NPs exhibit an almost linear increase of fluorescence intensity (∼14% increase) in the temperature range of 20−32 °C, which is almost stabilized above ∼32 °C; whereas for P(NIPAM-*co*-NBDAE)-*b*-P(NIPAM-*co*-SPMA) brush-coated silica NPs, fluorescence intensity exhibits a continuous increase (∼20% increase) in the broad temperature range of 20−37 °C. As both types of polymer brushes contain P(NIPAM-*co*-NBDAE) sequences, the much broader phase transition range for P(NIPAM-*co*-NBDAE)-*b*-P(NIPAM-*co*-SPMA) brushes should be due to its higher grafted chain lengths (Scheme 2). It is worth noting that the enhancement of NBDAE fluorescence emission at elevated temperatures is advantageous for the more prominent FRET process, as the FRET efficiency is expected to be improved by the thermo-induced collapse of polymer brushes.

Figure 8a shows the fluorescence spectra obtained for the aqueous dispersion of hybrid silica nanoparticles coated with P(NIPAM-*co*-NBDAE)-*b*-P(NIPAM-*co*-SPMA) brushes upon UV irradiation in the temperature range of 20−37 °C. Upon heating, the fluorescence
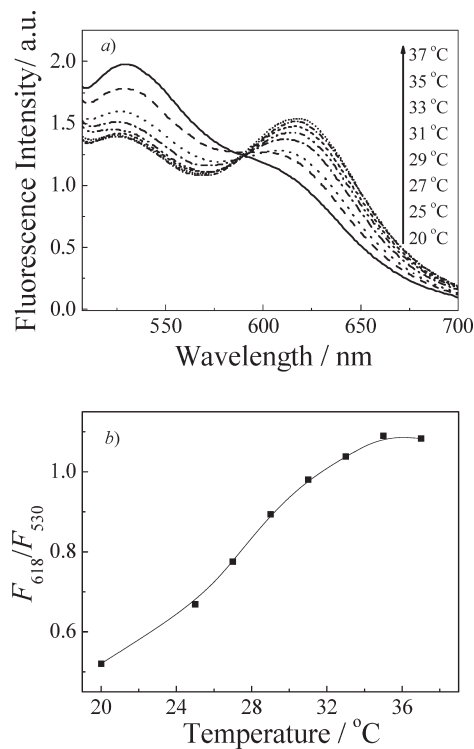
intensity of NBDAE fluorescence emission at 530 nm appreciably decreases, whereas the emission intensity of the MC form of SPMA residues at 618 nm increases, affording an increased fluorescence intensity ratio, F_{618}/F_{530}, with the temperature increase (Figure 8b). Visual inspection by the naked eye also reveals an apparent thermo-induced change from orange to red fluorescence emission transition for the hybrid NP dispersion upon UV 365 nm irradiation (Scheme 2b). As FRET donors (NBDAE moieties) and acceptors (SPMA residues in the MC form) are expected to randomly distribute within the inner and outer layers of polymer brushes, respectively, there is a distribution of FRET efficiencies between different donor−acceptor species of varying spatial distances within hybrid nanoparticles. Thus, there are always donor and acceptor pairs with the spatial distance falling into the range of the Förster radius and the FRET process between NBDAE moieties and MC residues will occur irrespective of temperatures. Moreover, fluorescence emission at ∼618 nm is a sum of contributions from the FRET process and the direct excitation of SPMA residues in the MC form by the incident light; however, it is quite difficult to quantify the relative contribution from both factors. For simplicity, the average FRET efficiency can be roughly estimated as $E = 1 - F/F_0$, where F and F_0 are the NBDAE donor fluorescence intensity of hybrid nanoparticle dispersion at 530 nm upon UV and vis irradiation at a given temperature, respectively. Thus, the average FRET

Article

Chem. Mater., Vol. 21, No. 16, 2009 3797

efficiency at 20 and 37 °C are determined to be 36% and 62%, respectively.

On the basis of LLS results, hybrid silica NPs coated with P(NIPAM-*co*-NBDAE)-*b*-P(NIPAM-*co*-SPMA) brushes exhibit an thermo-induced collapse from 85 nm at 20 °C to 62 nm at 37 °C (Figure 3). Considering that silica cores possess a radius of 45 nm, we can roughly estimate that the NBDAE-labeled inner layer and SPMA-labeled outer layer possess thicknesses of 10.9 and 29.1 nm at 20 °C and 4.6 and 12.4 nm at 37 °C, respectively. The Förster radius, R_0, between NBD and SPMA residues can be estimated to be ∼4 nm, as reported by Wu and co-workers.[33] As effective energy transfer can only occur in the range of $R_0 \pm 0.5R_0$, the upper limit of distance between donor and acceptor species for effective FRET processes is ∼6 nm. This can explain well the enhanced FRET efficiency between NBDAE and SPMA residues located within the inner and outer layers of P(NIPAM-*co*-NBDAE)-*b*-P(NIPAM-*co*-SPMA) brushes upon heating. It is noteworthy that even for the collapsed polymer brushes at 37 °C, the FRET process between certain NBDAE moieties in the inner layer (4.6 nm thickness) and SPMA residues in the outer layer (12.4 nm thickness) cannot occur due to having a spatial separation of more than 6 nm. Thus, it is reasonable to achieve a FRET efficiency of 62% for hybrid nanoparticles with fully collapsed P(NIPAM-*co*-NBDAE)-*b*-P(NIPAM-*co*-SPMA) diblock polymer brushes at elevated temperatures.

On the basis of the results shown in Figure 8b, hybrid NPs coated with P(NIPAM-*co*-NBDAE)-*b*-P(NIPAM-*co*-SPMA) brushes exhibit a thermo-induced increase of fluorescence intensity ratios, F_{618}/F_{530}, from 0.52 at 20 °C to 1.08 at 37 °C. Thus, this novel type of hybrid NPs can serve as excellent ratiometric fluorescent thermometers. Moreover, the detectable temperature range with sensitive signal changes can be further turned by adjusting the phase transition range via the copolymerization of hydrophilic or hydrophobic comonomers into PNIPAM brushes.

It has been previously established that PNIPAM brushes grafted at the surface of spherical nanoparticles exhibit a two-stage collapse upon heating, and the first one can extend to temperatures well below the LCST of free PNIPAM chains in aqueous solution.[36,55,59,60] To further confirm this, we also investigated the temperature-dependent FRET efficiency for the aqueous solution of P(NIPAM-*co*-NBDAE)-*b*-P(NIPAM-*co*-SPMA) chains cleaved from hybrid silica NPs, and the results are shown in Figure 9. Interestingly, we can only observe the considerable increase of F_{618}/F_{530} at ∼31 °C for free P(NIPAM-*co*-NBDAE)-*b*-P(NIPAM-*co*-SPMA) chains in aqueous solution (Figure 9b). A direct comparison between Figures 8b and 9b clearly revealed that P(NIPAM-*co*-NBDAE)-*b*-P(NIPAM-*co*-SPMA)
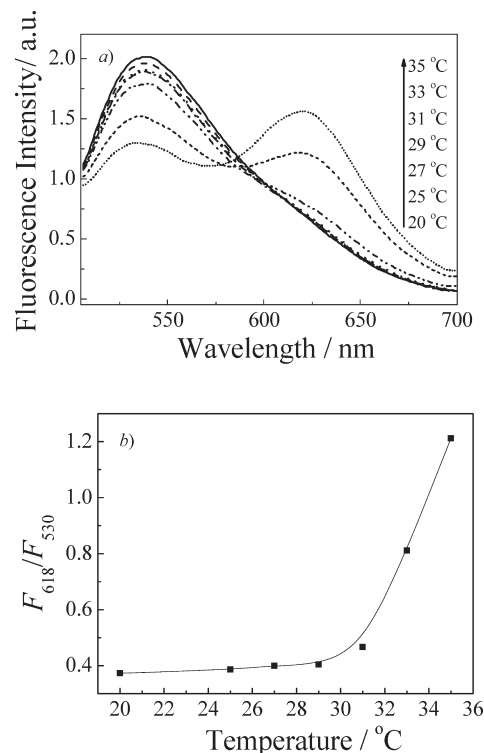
(59) Luo, S. Z.; Xu, J.; Zhu, Z. Y.; Wu, C.; Liu, S. Y. *J. Phys. Chem. B* **2006**, *110*, 9132–9139.
(60) Zhang, Y. F.; Luo, S. Z.; Liu, S. Y. *Macromolecules* **2005**, *38*, 9813–9820.

Figure 9. (a) Fluorescence spectra (λ_{ex} = 480 nm; slit widths: ex 4 nm, em 4 nm) and (b) fluorescence intensity ratio changes, F_{618}/F_{530}, in the temperature range of 20−37 °C obtained for the aqueous solution (0.05 g/L) of P(NIPAM-*co*-NBDAE)-*b*-P(NIPAM- *co*-SPMA) chains cleaved from hybrid silica nanoparticles. All spectra were recorded immediately after 365 nm UV irradiation for 4 min.

polymer brushes exhibit a much broader thermal phase transition, as compared to free chains in aqueous solution. Another point that needs to be considered is that within the inner and outer layers of diblock brushes labeled with NBDAE and SPMA moieties, respectively, dye contents are quite low (∼0.3 and 0.15 mol %), and the probability for the same diblock chain to bear both the NBDAE donor and SPMA acceptor is quite low considering an overall DP of ∼200. Thus, for both diblock copolymer brushes and free diblock chains, the interchain FRET process will dominate compared to the intrachain FRET process. As regards the latter, prominent FRET can only be observed in the aggregation state above the LCST; whereas for diblock brushes, the grafting topology is advantageous for the interchain FRET process due to the close spatial proximity of the donor and acceptor species.

Conclusion

In summary, hybrid silica nanoparticles densely grafted with thermoresponsive poly(*N*-isopropylacrylamide) (PNIPAM) brushes with inner and outer layers selectively labeled with fluorescence resonance energy transfer (FRET) donors, 4-(2-acryloyloxy-ethylamino)-7-nitro-2,1,3-benzoxadiazole (NBDAE), and photoswitchable acceptors, 1′-(2-methacryloxyethyl)-3′,3′-dimethyl-6-nitro-spiro(2*H*-1-benzo-pyran-2,2′-indoline) (SPMA), respectively, via surface-initiated sequential atom transfer radical polymerization (ATRP). UV irradiation of the

aqueous dispersion of hybrid silica nanoparticles induces the transformation of SPMA moieties in the outer layer of polymer brushes from the nonfluorescent spiropyran (SP) form to the fluorescent merocyanine (MC) form, leading to occurrence of the FRET process between NBDAE and SPMA residues. Most importantly, the FRET efficiency can be facilely tuned via thermo-induced collapse/swelling of P(NIPAM-*co*-NBDAE)-*b*-P(NIPAM-*co*-SPMA) brushes by changing the relative distance between the donor and acceptor species located within the inner and outer layers of polymer brushes, respectively. On the other hand, when the hybrid nanoparticle dispersion was irradiated with visible light again after UV irradiation, the MC form of SPMA moieties reverts back to the nonfluorescent SP form, leading to turning off the FRET process. Overall, an aqueous dispersion of this novel type of hybrid silica nanoparticles is capable of emitting multicolor fluorescence, which can be facilely tuned by UV irradiation, visible light, and temperatures or a proper combination of these factors.

Supporting Information Available: Figures S1−S4. This material is available free of charge via the Internet at http://pubs.acs.org.